JOURNAL OF AIRCRAFT
Vol. 39, No. 1, January–February 2002

Engineering Notes

ENGINEERING NOTES are short manuscripts describing new developments or important results of a preliminary nature. These Notes cannot exceed 6 manuscript pages and 3 figures; a page of text may be substituted for a figure and vice versa. After informal review by the editors, they may be published within a few months of the date of receipt. Style requirements are the same as for regular contributions (see inside back cover).

Three-Dimensional Wing Flow Computations Using Implicit Weno Euler Solvers

Jaw-Yen Yang,* Ruey-Hor Yen,† and Yeu-Ching Perng‡
National Taiwan University,
Taipei 10764, Taiwan, Republic of China

Introduction

IN this Note three-dimensional inviscid flows over wings are calculated by solving the Euler equations using implicit weighted ENO schemes. The Weighted Essentially Non-Oscillatory (WENO) schemes proposed recently by Liu et al.[1] and extended by Jiang and Shu[2] can achieve good convergence property while keeping the robustness and high-order accuracy of ENO[3,4] schemes. The main idea of ENO scheme is to select the smoothest stencil among several competing candidates to approximate the fluxes to a high-order accuracy and meanwhile to avoid oscillations near discontinuities. However, the freely adaptive stencil is not necessary in smooth solution region, and it could change even by a round-off perturbation near zeroes of the solution and its derivatives.[1,2] Numerical experiments with implicit ENO schemes usually suffer slow and even stagnant convergence rate for steady-state solution computations because of this adaptive stencil. Besides, the stencil-choosing step involves frequent usage of logical statements, which perform poorly on vector machines.

In Ref. 5 a class of implicit WENO schemes for the Euler equations has been successfully applied to two-dimensional airfoil flows. Good convergence rate to steady-state solution has been illustrated. To improve the efficiency and convergence to the steady state, the lower-upper symmetric Gauss–Seidel (LU-SGS) implicit algorithm[6] is adopted. LU-SGS scheme is not only unconditionally stable but also completely vectorizable in any dimensions. The resulting implicit LU-SGS WENO schemes for the Euler equations have several desirable features. They are more accurate, less dissipative, and have good convergence rate to steady-state solutions, thus rendering them good candidate for Euler simulations, particularly when compared with the implicit ENO counterpart. The details of the present scheme are similar to those given in Ref. 5 except that here we extend it to three space dimensions. Several numerical issues regarding to three-dimensional Euler computations have been reported such as the effects of numerical dissipation, inconsistent coarse and fine grid solutions, local and global minimum time stepping, and Kutta conditions.[7,8] The aim of this work is to use implicit WENO Euler solver to tackle these numerical issues by solving several three-dimensional Euler flows. The computations are performed for the subsonic flow over NACA 0015 rectangular wing, transonic flow over ONERA M6 wing, and supersonic flow over elliptic delta wing.

Received 20 November 1999; revision received 6 August 2001; accepted for publication 12 August 2001.

*Professor, Institute of Applied Mechanics; yangjy@spring.iam.ntu.edu.tw. Member AIAA.
†Professor, Department of Mechanical Engineering.
‡Ph.D. Student, Department of Mechanical Engineering.

Results and Discussion

Subsonic Flow over NACA 0015 Wing

The first computation is subsonic flow over a rectangular platform, untwisted, cantelevered NACA 0015 wing with aspect ratio 3.3. Computations were performed at $M_\infty = 0.18$ and $\alpha = 12.44$ deg, where M_∞ is the freestream Mach number and α is the angle of attack. The grid system is O-O type grid with $129 \times 26 \times 45$ grid points. The outer boundaries were extended to 20 chord lengths in all directions. The first grid line is at a distance of 10^{-3} chord length off the wall.

The solutions were calculated using WENO2-Roe and ENO2-Roe schemes at local Courant–Friedrichs–Lewy (CFL) number 15.0. The computations with present code were compared with three-dimensional upwind Euler code developed by Barth[9] as well as with the wind-tunnel experiments carried out by McAlister and Takahashi.[10] Pressure distribution is graphed in Fig. 1. The results of WENO2-Roe and ENO2-Roe schemes are almost the same. The comparison of results with both Barth code and experiment is extremely good. The present codes appear to resolve the suction pick slightly better than the Barth code and more accurate at near wing tip location. Figure 2 shows the convergence histories for WENO2 and ENO2 schemes. After the residuals have decayed for two orders of magnitude, the convergence of ENO2-Roe scheme is leveling off because of the freely adaptive stencil, whereas monotone convergence is achieved with WENO2-Roe scheme. A drop of six orders of magnitude of the l_2 norm can be attained in 3000 iterations.

Transonic Flow over ONERA M6 Wing

The second computation is transonic flow over the ONERA M6 wing at $M_\infty = 0.8395$, $\alpha = 3.06$ deg. The ONERA M6 wing is a

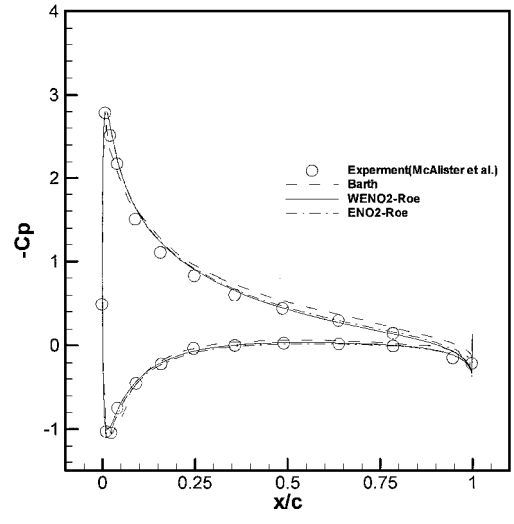

Fig. 1 Steady pressure distributions for NACA 0015 rectangular wing at $M_\infty = 0.18$, $\alpha = 12.44$ deg and $y/b = 0.8989$.

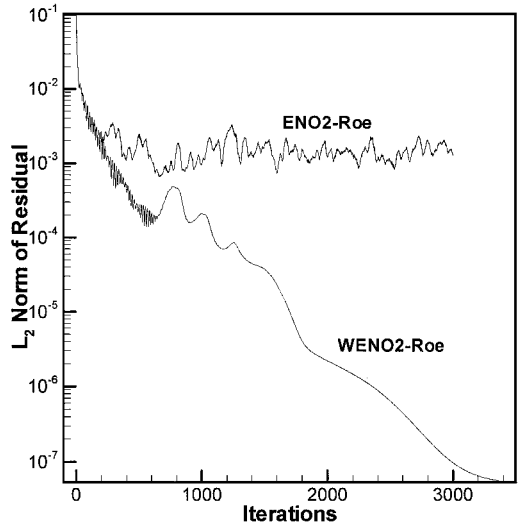

Fig. 2 Convergence history for NACA 0015 rectangular wing at $M_\infty = 0.18$ and $\alpha = 12.44$ deg.

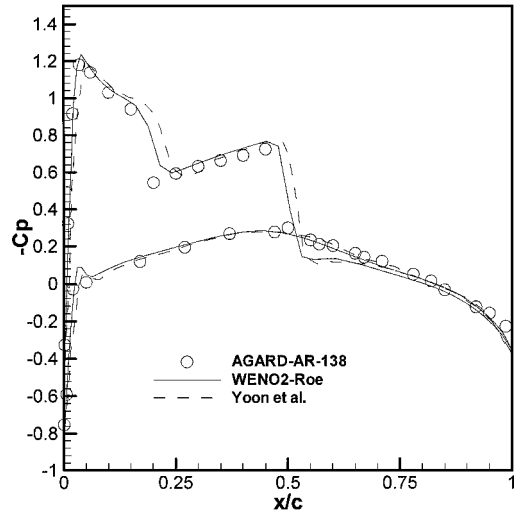

Fig. 3 Steady pressure distributions for ONERA M6 wing at $M_\infty = 0.8395$, $\alpha = 3.06$ deg, and $y/b = 0.65$.

symmetric airfoil section with a sweep angle of 30 deg. The wing is tapered with a taper ratio of 0.56 and has an aspect ratio of 3.8. The airfoil section is an ONERA D symmetric section with 0.1 maximum thickness-to-chord ratio. Extensive wind-tunnel test data exist for the ONERA M6 wing, in particular pressure data for transonic flow conditions.[11]

Our calculation is performed on an O-O-type grid system containing $161 \times 26 \times 45$ grids in the wrap-around, spanwise, and body-normal directions, respectively. The outer boundaries were extended to 30 chord lengths in all directions. The first grid line is at a distance of 10^{-3} chord length off the wall. The solutions were calculated using WENO2-Roe scheme at local CFL number 20.0. In Fig. 3 we show the pressure coefficients of present scheme as compared with the experimental data [11] and the other calculations by Yoon et al.[12] in which the number of grid points used were $191 \times 33 \times 49$. The results of Yoon et al.[12] were obtained using artificial diffusions scheme with a LU-SGS implicit method. It is shown that results of WENO2-Roe scheme are in good agreement with the experimental data and are more accurate than the results of Yoon et al. as better representations of shock-wave profiles and locations can be observed for the WENO scheme. Figure 4 shows a view of the pressure contours along the upper surface. The configuration obviously results in the lambda double-shock pattern for transonic flow on a swept wing, where the two shocks coalesce to form a single shock near the wing tip.

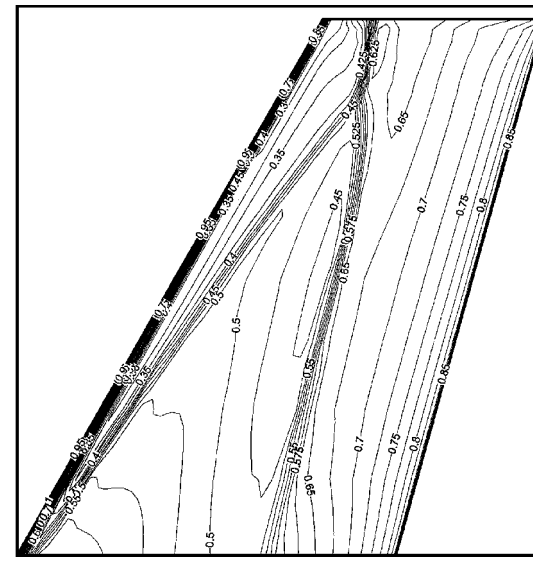

Fig. 4 Upper surface pressure contours for ONERA-M6 wing at $M_\infty = 0.8395$ and $\alpha = 3.06$ deg.

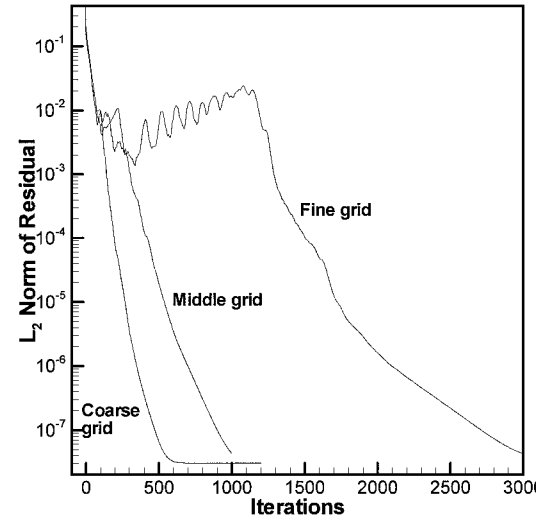

Fig. 5 Convergence history for elliptic delta wing at $M_\infty = 2.0$ and $\alpha = 10$ deg. A comparison of different grid system.

Supersonic Flow over Elliptic Delta Wing

The supersonic case is an inviscid flow over an elliptic delta wing with half-angles 20 and 1.5 deg in the lateral and vertical directions. This geometry provides a realistic approximation to a sharp leading edge while maintaining a continuous curvature in the tip region. The freestream conditions are Mach number 2.0 and angle of attack 10 deg.

Our solutions were calculated using WENO2-Roe scheme at local CFL number 20.0. Calculations were made on three different grids. The three grid systems are $(11 \times 61 \times 65)$, $(11 \times 121 \times 65)$, and $(11 \times 151 \times 65)$, with the minimum spacing normal to the wall surface $\Delta s/x = 0.005$, 0.0005, and 0.0002, respectively. At the wing vertex and the outer boundary of conical grid, freestream conditions are specified. The downstream station is located at $x = 1$, and the boundary conditions there are extrapolated from the upstream station.

Figure 5 shows the convergence histories of the three different grid systems. Good convergence rate to steady-state solution has been illustrated for all grid systems, but the convergence history of fine grid contains a flowfield evolution process.[13] In Fig. 6 the iterative history of the pressure distributions using fine grid system is shown to illustrate this evolution process. Early in the calculation a crossflow shock forms on the leeside of wing near the tip. A vortex forms behind the shock creating a separated flow, which pushes

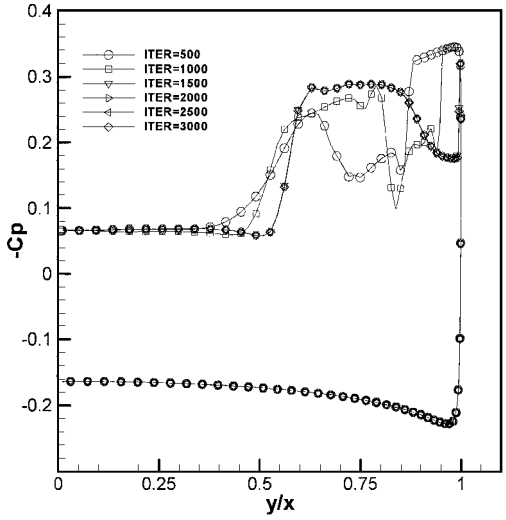

Fig. 6 Pressure distributions of fine grid for elliptic delta wing at $M_\infty = 2.0$ and $\alpha = 10$ deg, $x = 0.75$. A comparison of different iteration numbers.

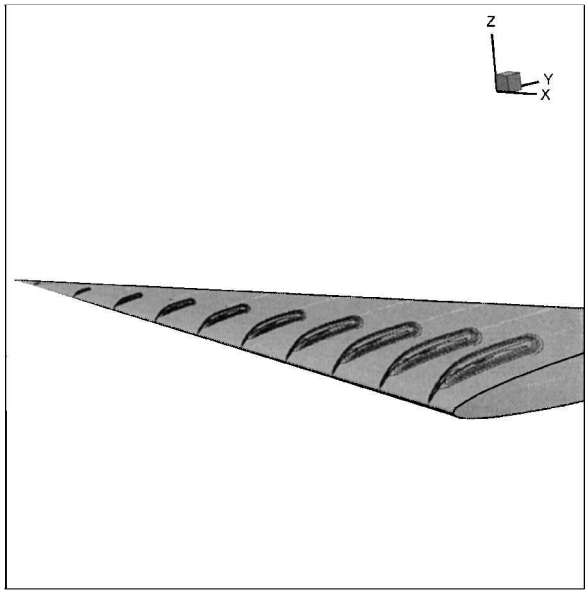

Fig. 7 Perspective view of the spanwise total-pressure contour of fine grid for elliptic delta wing at $M_\infty = 2.0$ and $\alpha = 10$ deg.

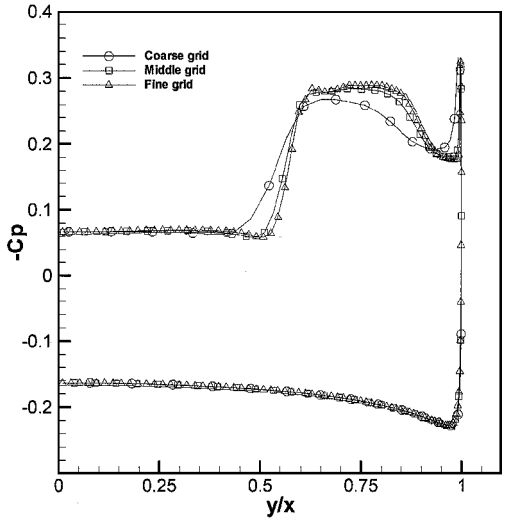

Fig. 8 Pressure distributions for elliptic delta wing at $M_\infty = 2.0$ and $\alpha = 10$ deg, $x = 0.75$. A comparison of different grid system.

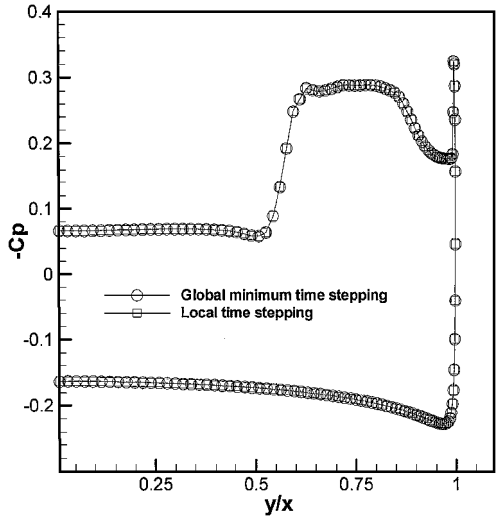

Fig. 9 Pressure distributions of fine grid for elliptic delta wing at $M_\infty = 2.0, \alpha = 10$ deg, $x = 0.75$. A comparison of different time stepping.

the crossflow shock outboard toward the wind tip. As the crossflow shock moves outboard, its strength decreases, and at the wing tip it collapses into a singular point. This leaves a leeside flowfield containing a large vortex. A perspective view of the spanwise total-pressure contour plot is shown in Fig. 7. A comparison of pressure coefficients for the three grid systems is given in Fig. 8, which indicates the flow is grid resolved. This also serves as a grid convergence check for the present method.

Our solutions obtained so far are based on the local time stepping because of its computational efficiency. Chakravarthy and Ota claimed that the separated flow solution was caused by the local time stepping. The next issue we address here is the effect of using global-minimum time stepping. Figure 9 shows that global-minimum time stepping produces the same solutions as that obtained using local time stepping.

Conclusions

High-resolution implicit WENO Euler codes for solving three-dimensional wing flows have been developed. The present method is based on weighted nonoscillatory spatial operator for convective flux. The time integration of equation is done using the implicit LU-SGS algorithm. Applications to subsonic flow over NACA 0015 rectangular wing, transonic flows over ONERA M6 wing, and supersonic flow over elliptic delta wing have been carried out to validate and illustrate the code. It is found that the present implicit WENO Euler solver can achieve much better convergence rate for steady-state calculations as compared with the implicit ENO counterpart. For NACA 0015 wing and ONERA M6 wing the solutions of the present algorithms compare well with the experimental data and other numerical results. The results for elliptic delta wing show that they are consistent with all grid sizes and the solutions are independent of the way time stepping is taken. Both local time stepping and global minimum time stepping produce the same solutions. Regarding the various issues of preceding three-dimensional Euler computations such as numerical dissipation of different schemes, inconsistent coarse and fine grid solutions, different time stepping, the present implicit WENO Euler solvers seem to provide a viable tool to produce accurate, less dissipative, and consistent solutions for the inviscid compressible wing flows over a broad range of Mach numbers.

Acknowledgment

This work was done under the auspicy of National Science Council, Taiwan, through Grants NSC-87-2212-E002-071 and NSC-88-2213-E002-026.

References

[1] Liu, X.-D., Osher, S., and Chan, T., "Weighted Essentially Nonoscillatory Schemes," *Journal of Computational Physics*, Vol. 115, No. 1, 1994, pp. 200–212.

[2]Jiang, G.-S., and Shu, C.-W., "Efficient Implementation of Weighted ENO Schemes," *Journal of Computational Physics*, Vol. 126, No. 1, 1996, pp. 202–228.

[3]Harten, A., Engquist, B., Osher, S., and Chakravarthy, S., "Uniformly High-Order Accurate Nonoscillatory Scheme, III," *Journal of Computational Physics*, Vol. 71, No. 2, 1987, pp. 231–303.

[4]Shu, C.-W., and Osher, S., "Efficient Implementation of Nonoscillatory Shock Capturing Schemes," *Journal of Computational Physics*, Vol. 77, No. 2, 1988, pp. 439–471.

[5]Perng, Y. C., Yen, R. H., and Yang, J. Y., "Implicit Weighted ENO Schemes for the Euler Equations," *Computational Fluid Dynamics Journal*, Vol. 8, No. 3, 1999, pp. 216–227.

[6]Yoon, S., and Jameson, A., "Lower-Upper Symmetric-Gauss-Seidel Method for the Euler and Navier–Stokes Equations," *AIAA Journal*, Vol. 26, No. 8, 1988, pp. 1025, 1026.

[7]Chakravarthy, S. R., and Ota, O. K., "Numerical Issues in Computing Inviscid Supersonic Flow over Conical Delta Wing," AIAA Paper 86-0440, Jan. 1986.

[8]Kandil, O. A., and Chuang, A., "Influence of Numerical Dissipation on Computational Euler Solutions for Conical Vortex Dominated Flows," *AIAA Journal*, Vol. 25, No. 6, 1987, pp. 1426–1434.

[9]Barth, T. J., "A 3-D Upwind Euler Solver for Unstructured Meshes," 10th AIAA Computational Fluid Dynamics Conf., AIAA Paper 91-1548-CP, June 1991.

[10]McAlister, K. W., and Takahashi, R. K., "NACA 0015 Wing Pressure and Trailing Vortex Measurements," USAAVSCOM TR-91-A-003, NASA Ames Research Center, CA, March 1991.

[11]Schmitt, V., and Charpin, F., "Pressure Distributions on the ONERA-M6 Wing at Transonic Mach Numbers," AGARD-AR-138- B1, NATO, Aug. 1979.

[12]Yoon, S., Jameson, A., and Kwak, D., "Effect of Artificial Diffusion Schemes on Multigrid Convergence," 12th AIAA Computational Fluid Dynamics Conf., AIAA Paper 95-1670-CP, June 1995.

[13]Wardlaw, A. B., Jr., and Davis, S. F., "Euler Solutions for Delta Wings," *AIAA Journal*, Vol. 28, No. 7, 1990, pp. 1826–1829.

Propeller Momentum Theory with Slipstream Rotation

W. F. Phillips*
Utah State University, Logan, Utah 84322-4130

Introduction

ONE critical component of propeller blade element theory[1] is the prediction of the velocity induced on the propeller disk as a result of the lift developed by the blades. Two methods are commonly used to predict this induced velocity. The most comprehensive method is Goldstein's vortex theory.[2] The simplest method is propeller momentum theory,[3–5] which is the topic addressed here. The major objection to the use of classical propeller momentum theory has been its failure to account for the rotation of the fluid within the slipstream.

Classical propeller momentum theory is presented in most aeronautical engineering textbooks that deal with propeller performance.[3–5] Momentum theory is based on the hypothesis of a streamtube, which encloses the complete propeller disk as shown in Fig. 1. This streamtube is assumed to extend from a plane infinitely far upstream from the propeller disk to a plane infinitely far downstream. All of the fluid that enters this streamtube on the far upstream side must pass through the propeller disk and exit the streamtube on the far downstream side.

Received 22 February 2001; revision received 1 October 2001; accepted for publication 7 October 2001.

*Professor, Mechanical and Aerospace Engineering Department, 4130 Old Main Hill. Member AIAA.

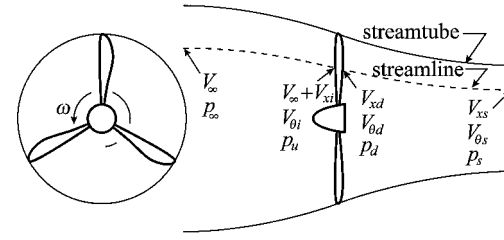

Fig. 1 Momentum theory model for the pressures and velocities of the fluid that flows through the disk of a rotating propeller, including the effects of fluid rotation.

In addition to the foundation hypothesis of streamtube flow shown in Fig. 1, classical propeller momentum theory imposes five simplifying approximations. The flow is assumed to be 1) inviscid and 2) incompressible; 3) all rotation of the fluid within the streamtube is neglected; and both 4) the velocity and 5) the static pressure are assumed uniform over each cross section of the streamtube. With these approximations the induced velocity V_i is expressed as a function of the freestream velocity V_∞ and the thrust T. In dimensionless form the result is

$$\frac{V_i}{(\omega/2\pi)d_p} = \sqrt{\frac{J^2}{4} + \frac{2C_T}{\pi}} - \frac{J}{2} \tag{1}$$

where $C_T \equiv T/[\rho(\omega/2\pi)^2 d_p^4]$ and $J \equiv V_\infty/[(\omega/2\pi)d_p]$ are the usual thrust coefficient and advance ratio. Here, ω is used to represent the propeller angular velocity, d_p is the propeller diameter, and ρ is the fluid density. From the same analysis the propulsive efficiency for the propeller is found to be

$$\eta_i \equiv TV_\infty/Q\omega = \left(\tfrac{1}{2} + \sqrt{\tfrac{1}{4} + 2C_T/\pi J^2}\right)^{-1} \tag{2}$$

where Q is the torque required to turn the propeller and η_i is usually called the ideal propulsive efficiency.

The major objection to these results has been the failure of the method to account for rotation of the fluid within the slipstream. There appears to be no physical basis for neglecting slipstream rotation. Clearly, torque must be applied to turn the propeller and that torque must result in rotation of the fluid within the slipstream. Because some of the power supplied to the propeller must go to support this rotation, the propulsive efficiency will be reduced as a result of slipstream rotation. In the following analysis we shall examine the magnitude of this effect.

Effects of Slipstream Rotation

We shall now consider the incorporation of the angular momentum equation into the model hypothesized in propeller momentum theory. To isolate the effects of slipstream rotation, we will continue with the assumptions of inviscid, incompressible, uniform flow, but we will now allow for rotation of the fluid within the streamtube. Accordingly, we will continue to assume the existence of a streamtube, which encloses the complete propeller disk as shown in Fig. 1. This streamtube is still assumed to extend infinitely far upstream from the propeller disk, to a plane where the static pressure is constant and equal to the freestream static pressure p_∞. In this plane the axial velocity is the freestream velocity V_∞, and there is no circumferential velocity. Likewise, the streamtube is assumed to extend infinitely far downstream from the propeller disk to a plane where the velocity in the slipstream is no longer changing in the axial direction. Consistent with the uniform flow assumption used in classical propeller momentum theory, we will continue to assume uniform axial velocity but will now allow for a uniform angular velocity as well. Because we wish to examine the effect of slipstream rotation on the results predicted by propeller momentum theory, at first thought one might be tempted to continue with the assumption of uniform pressure, which is also imposed in classical propeller momentum theory. However, this assumption is not consistent with rotation in the ultimate slipstream.